Correlated Structures in a Balanced Motion Interacting with an Internal Wave

Igor Maingonnat, Gilles Tissot, Noé Lahaye

Correlated structures in a balanced motion interacting with an internal wave

Igor Maingonnat, Gilles Tissot, Noé Lahaye

INRIA Rennes Bretagne Atlantique, IRMAR – UMR CNRS 6625, av. General Leclerc, 35042 Rennes, France

December 2022

Abstract

Characterizing the loss of coherence of an internal tide propagating through mesoscale turbulence has been a major challenge in oceanography, particularly due to its implications for the interpretation of satellite data. In this paper, we intend to study the correlations between a balanced motion and the incoherent part of a wave in an idealised configuration. We introduce a new modal decomposition technique, named broad-band proper orthogonal decomposition (BBPOD), which consists in performing a proper orthogonal decomposition (POD) on complex demodulated variables. After connecting BBPOD to the standard SPOD, we show that BBPOD, coupled with the extended POD technique enables us to associate the principal components of the incoherent field to the slow flow structures responsible of this loss of coherence through triadic interactions with the incident wave.

Keywords: Internal tide interactions, spectral proper orthogonal decomposition, broad-band proper orthogonal decomposition.

1 Introduction

Internal tides, generated by interactions between the barotropic tide and topographic features such as ridges or continental slopes, are ubiquitous in the ocean, playing a crucial role in vertical mixing and energy transport. They propagate over large distances, encountering regions with energetic mesoscale turbulence, and they lose their fixed phase relationship with the astronomical forcing, a phenomenon known as incoherence. This loss of coherence, highly unpredictable, complicates for example our ability to disentangle internal tides and low-frequency turbulent signals from satellite data (Richman et al. 2012).

To face these difficulties, there have been various studies to better understand and predict the impact of a balanced (turbulent) jet on the inertia-gravity wave field properties. For instance, Savva and Vanneste (2018) and Ward and Dewar (2010) studied the internal tide scattering. Ponte and Klein (2015) examined the incoherence time scales for different turbulent configura-

tions, and Dunphy et al. (2017) quantified the interaction terms via vertical-mode projection of the linearized Boussinesq equations.

We consider in the present paper a data-driven approach to study from idealised numerical simulations, the structures of the jet, which are correlated with the incoherent contributions of the wave field. Extracting coherent structures from a data set can be performed in the spectral domain by spectral proper orthogonal decomposition (SPOD) (Towne et al. 2018). Some attempts to connect these reduced features with non-linear interactions have been proposed for instance in Karban et al. (2022) by identifying the contribution of the non-linear term correlated with the SPOD mode through extended proper orthogonal decomposition (EPOD, Boree (2003)). Unfortunately, non-linear forcing is a quantity more difficult to interpret and associate with physical mechanisms than a pressure or velocity field for instance. We propose instead a new *broad-band proper orthogonal decomposition (BBPOD),* derived from the SPOD. By taking advantage of the strong time scale separation between the two dynamics and considering small-amplitude wave, this formulation allows us to connect the non-linear interactions between the slow motions of the jet and the incoherent contributions of the wave through the EPOD method. The non-linear interactions are here understood as triadic interactions with the slow motion that will lead to a broadband frequency structure of the incoherent wave field.

The plan is as follows. We will begin by describing the model used for our simulations in section 2. In section 3.1, the original SPOD method is reviewed and a connection to the proposed BBPOD method is made (section 3.2). Sections 4 and 5 will summarize the study and bring some perspectives.

2 Model

The propagation of internal tides through a nearly-balanced jet is examined in a one layer rotating shallow water (RSW) model. The equations are non-dimensionalized as follows. The characteristic time-scale is the inertial time $T = f^{-1}$, inverse of the Coriolis frequency. The reference length scale L is chosen to be of the order of the jet thickness, taken equal to the first Rossby radius of deformation R_d, such that the Burger number $B_u = R_d^2/L^2$ is equal to one. A beta-plane approximation, with parameter β, accounts for the effect of rotation, and a radiative damping term α is added on the continuity equation, (following *e.g.* Brunet and Vautard 1996). Adequat artificial hyperviscosity, consistent with energy dissipation and conservation of angular momentum, is also used (see Ochoa et al. 2011).

Let Ω be a bounded subset of $\mathbb{R}^2$, the equations without viscosity, defined on $\Omega \times \mathbb{R}_+$, are

$$\partial_t h + B_u \text{div } \mathbf{v} + R_o((\mathbf{v}\cdot\nabla)h + h \text{ div } \mathbf{v}) = -\alpha h \tag{1}$$

$$\partial_t \mathbf{v} + (1+\beta y)\boldsymbol{v}^\perp + R_o(\mathbf{v}\cdot\nabla)\mathbf{v} = -\nabla h, \tag{2}$$

where $\mathbf{v} = (u, v)$ is the horizontal velocity, $\boldsymbol{v}^\perp = (-v, u)^T$, h is the sea surface height (SSH) anomaly and $R_o = U/(fL)$ is the Rossby number.

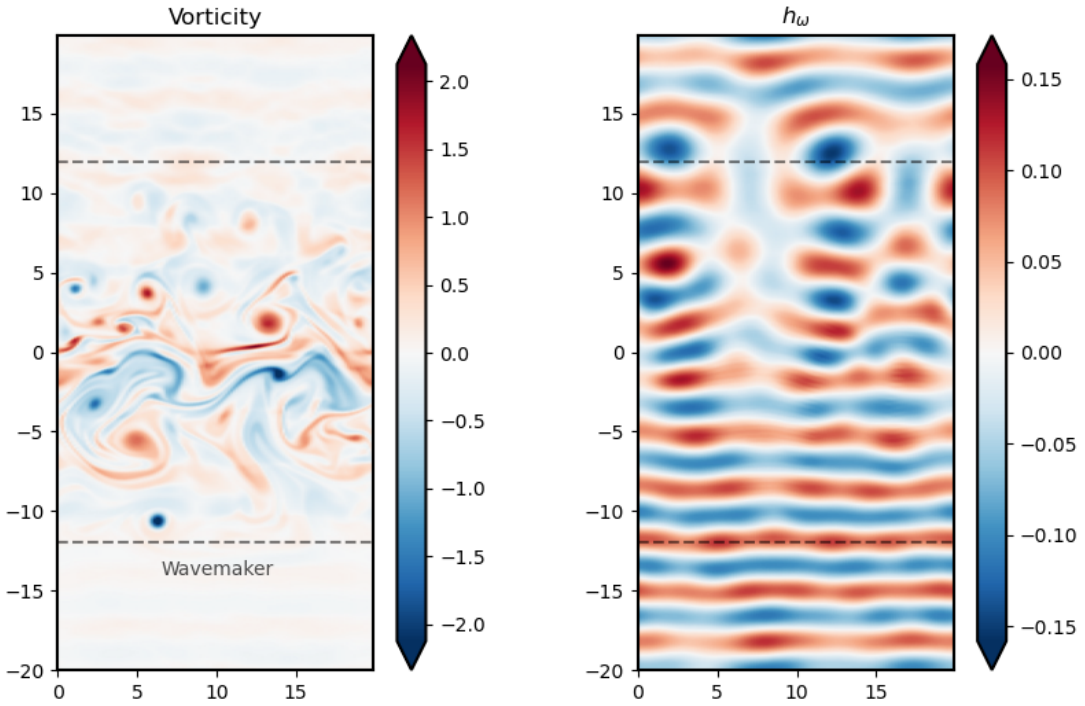

Figure 1: A snapshot taken from the RSW simulation. On the left the vorticity field and on the right the internal wave SSH anomaly h_ω, extracted by bandpass filtering centered around the wave frequency $\omega = 2$.

A numerical simulation of system (1)-(2) of a plane wave interacting with a zonal jet has been performed. Equations have been discretized by a pseudo-spectral method and with a Runge-Kutta time-scheme using the code Dedalus (Burns et al. 2020). The domain Ω is a doubly periodic rectangular domain of size $[0, 20] \times [-20, 20]$ discretized on a 128×512 grid. The simulation is initialized with an eastward zonal jet at geostrophic equilibrium with a small perturbation to trigger the instabilities. During the whole experiment, a northward propagating plane wave with frequency fixed at $\omega = 2$ is generated in a nudging layer in the South of the domain, and an eastward wind forcing is applied to maintain the balanced current. A spin-up phase allows the jet to evolve toward a statistically stationary state. The experiment continues with snapshots stored every 0.1 wave period, such that a sufficiently long series $\boldsymbol{q} = (u, v, h)^T$ of 12000 snapshots are collected, representing nearly 4000 wave periods. Note that a sufficient sampling in time is required for extracting the wave field by filtering in 3.2. An example of snapshot associated with one run of the simulation is shown in Figure 1.

This simple model can sustain waves interacting with a turbulent flow. Northward rotating shallow water waves are inertia gravity waves satisfying the dispersion relation

$$k_y^2 = \frac{\omega^2 - (1 + \beta y)^2}{B_u}, \tag{3}$$

with k_y denoting the spatial wavenumber in the meridional direction, which is function of the tidal frequency ω.

3 Methods

The methods to extract correlated structures in a flow field are described in this section. In the following we denote our state vector by $\boldsymbol{q} = (u, v, h)^T$.

3.1 Spectral proper orthogonal decomposition

Spectral proper orthogonal decomposition is an extension of POD methods (see Lumley 1967), and aims at extracting coherent structures in spectral space from numerical or experimental data. The data are assumed to be issued from a statistically stationary random process, which is verified thanks to the hypothesis of small-amplitude waves, such that the balanced flow is marginally impacted by the wave propagation. The modes obtained from this decomposition are space-time uncorrelated from each other.

We interpret our state vector as a zero-mean second order random process $\boldsymbol{q}$ (which can be obtained by subtracting the time averaged field beforehand) indexed over $\Omega \times \mathbb{R}^+$, a subset of spatio-temporal variables. Consider $\hat{\boldsymbol{q}}(\omega)$ the Fourier transform of the process at angular frequency ω. We assume that each realization of $\hat{\boldsymbol{q}}(\omega)$ belongs to $L^2_{\mathbf{W}}(\Omega, \mathbb{C}^3) = \{\boldsymbol{g} : \Omega \to \mathbb{C}^3, \int_\Omega \boldsymbol{g}^*(\boldsymbol{z})\mathbf{W}(\boldsymbol{z})\boldsymbol{g}(\boldsymbol{z})\,\mathrm{d}\boldsymbol{z} < \infty\}$, the ensemble of square integrable functions in space (periodic at boundary) relatively to a positive definite weight matrix $\mathbf{W}$: $\Omega \to M_n(\mathbb{R})$. The superscipt $\cdot^*$ denotes the transpose-conjugate operation. The matrix $\mathbf{W}$ is chosen such that the L^2-norm approximates the energy of the RSW model (1)-(2):

$$\|\boldsymbol{q}\|^2_{\mathbf{W}} = \frac{1}{2}\int_\Omega (1 + \lambda\bar{h})(u^2 + v^2)\,\mathrm{d}x\mathrm{d}y + \frac{1}{2B_u}\int_\Omega h^2\,\mathrm{d}x\mathrm{d}y, \tag{4}$$

where λ refers to the deviation of the isopycnal taken equal to R_o/B_u and $\bar{h}$ corresponds to the temporal-mean of SSH anomaly. The term $1 + \lambda\bar{h}$ is assumed to remain strictly positive (which is necessary for ensuring positiveness of the norm), since we do not consider zero or negative sea-surface height.

Let us recall briefly the basic principle of SPOD. By stationarity the auto-correlation function $\mathbf{C}(x, y, t, x', y', t') = \mathbb{E}(\boldsymbol{q}(x, y, t) \otimes \boldsymbol{q}^*(x', y', t'))$ satisfies :

$$\mathbf{C}(x, y, t, x, y, t') = \mathbf{C}(x, y, x', y', t - t'), \tag{5}$$

where $\otimes$ denotes the dyadic product of two vectors in $\mathbb{R}^3$. The objective of SPOD method is therefore to find a deterministic function $\boldsymbol{\psi}$ satisfying the Fredholm equation :

$$\int_\Omega \mathbf{S}(x, y, x', y', \omega)\mathbf{W}(x', y')\boldsymbol{\psi}(x', y', \omega)\,\mathrm{d}x'\mathrm{d}y' = \lambda(\omega)\boldsymbol{\psi}(x, y, \omega), \tag{6}$$

where $\mathbf{S}(x,y,x',y',\omega) = \int_{\mathbb{R}} \mathbf{C}(x,y,x',y',\tau)e^{-i\omega\tau}\,\mathrm{d}\tau$ is the cross spectral density matrix (CSD).

The Karhunen-Loeve theroem (Loève 1955) states that $\forall\omega \in \mathbb{R}$, equation (6) has an infinite number of solutions $(\lambda_j(\omega), \boldsymbol{\psi}_j(\omega))_{j=1}^{\infty}$ such that: $(\boldsymbol{\psi}_j(\omega))_{j=1}^{\infty}$ is an orthonormal basis in $L^2_{\mathbf{W}}(\Omega, \mathbb{C}^3)$ where we can expand the Fourier transform of the field into structures uncorrelated from each other:

$$\hat{\boldsymbol{q}}(x,y,\omega) = \sum_{j=1}^{\infty} a_j(\omega)\boldsymbol{\psi}_j(x,y,\omega) \tag{7}$$

with $\mathbb{E}(a_j(\omega)a_{j'}(\omega')) = \lambda_j(\omega)\delta_{j,j'}(\omega-\omega')$ and $\forall j,\ \lambda_j(\omega) \geq 0$. Moreover, a truncated expansion at order n will maximize the mean energy (defined by the norm $\|\cdot\|^2_{\mathbf{W}}$), compared to any other decomposition of the same order, and SPOD provides an optimal decomposition of the CSD:

$$\mathbb{E}(\|\hat{\boldsymbol{q}}(\omega)\|^2_{\mathbf{W}}) = \sum_{j=1}^{\infty} \lambda_j(\omega) \tag{8}$$

$$\mathbf{S}(x,y,x',y',\omega) = \sum_{j=1}^{\infty} \lambda_j(\omega)\boldsymbol{\psi}_j(x,y,\omega)\boldsymbol{\psi}_j^*(x',y',\omega). \tag{9}$$

Therefore, by solving the Fredholm equation at the tidal frequency, we are able to separate the fast from the slow component of the process by a spectral decomposition, expanded onto an orthonormal basis optimal energetically.

It can be remarked that when there is an homogeneous direction, it is possible to compute the Fredholm equation in spectral space with respect to this direction. Each wave-number can be computed independently, and each corresponding Fourier component is solution of the original Fredholm problem. For more complete description of SPOD (see Towne et al. 2018; Schmidt and Colonius 2020). In our case, the domain is homogeneous in the x direction, but we still consider the 2D problem for the physical relevance of the extended BBPOD problem presented in section (3.2).

3.2 Broadband proper orthogonal decomposition

The BBPOD consists in estimating by complex-demodulation (see Godfrey 1965) the correlation tensor of a band-passed-filtered signal, and its eigenfunctions. The associated algorithm is presented in this section. It will be compared with the Welch's method used in SPOD (see Welch 1967; Towne et al. 2018) and it will be shown that under some hypotheses both algorithms are equivalent. It can be noted that in Welch (1967), the connection with complex demodulation is briefly mentioned, and it is leveraged here with the computation of the eigenvectors and eigenvalues of the correlation tensor for a POD decomposition. We highlight by this equivalence, that due to windowing in the Welch's method, the features extracted by SPOD possess a spectral component with a thick frequency band. For the Broadband POD algorithm, this frequency band is explicit, and chosen through the definition of a filter. In the RSW model, the incoherent wave field possesses a broad band structure and Broadband POD allows us to obtain a complete decomposition of this field.

3.2.1 Complex demodulation of the wave field

Given a temporal series x_t, the principle of complex demodulation consists in the following computation :

$$x_d = \mathcal{L}(x_t e^{-i\omega t}), \tag{10}$$

where x_d is called the complex demodulated signal, $\mathcal{L}$ is a low-pass filter and ω is the demodulated frequency. Complex demodulation enables to extract the slowly varying amplitude envelop and phase deviations of the wave field. These variations are associated with wave incoherence.

First, we decompose the process $\boldsymbol{q}(x, y, t)$ in a sum of $\boldsymbol{q}_j(x, y, t)$ and $\boldsymbol{q}_\omega(x, y, t)$, representing the jet and wave contributions, respectively. The wave field can be expressed as:

$$\boldsymbol{q}_\omega(x, y, t) = \boldsymbol{q}_d(x, y, t)e^{i\omega t}, \tag{11}$$

where ω is the tidal frequency and $\boldsymbol{q}_d$ is a complex field slowly varying in time, accounting for the incoherence. The latter is then extracted by the complex demodulation of $\boldsymbol{q}$ (10), with a filter designed such that it isolates the slow variations of the background flow. As a consequence, through the $e^{-i\omega t}$ shift, the spectral-band of the extracted wave contains all effects of triadic interactions between the slow motions and the coherent wave. The jet contribution $\boldsymbol{q}_j$ is obtained by directly filtering $\boldsymbol{q}$ (zero frequency), including here the time-average. In this study, we assume that $\boldsymbol{q}$ is dominated by the superimposition of $\boldsymbol{q}_j$ and $\boldsymbol{q}_\omega$, which interact non-linearly. Note that for simplicity, a uniform time sampling of the data was chosen but this can be adapted to a non-uniform one, *e.g.* by interpolation on a regular grid or using filtering algorithms to irregular sampling.

3.2.2 Link with SPOD

For making the link with SPOD to estimate the CSD of a signal x_t, we write the temporal filter in a discrete form, with a time spacing Δt and $t_k = k\Delta t$. A wide class of linear filter can be expressed as the convolution:

$$\mathcal{L}(x_t) = \sum_{i=-m}^{m} b_i x_{t-i}, \tag{12}$$

where $(b_i)_{-m\leq i\leq m}$ are the discrete coefficients of the filter. Then,

$$(\mathcal{L}(x_t e^{-i\omega t}))_j = \sum_{k=-m}^{m} b_k x_{j-k} e^{-i\omega t_{j-k}} \tag{13}$$

$$= \sum_{k=j-m}^{j+m} b_{j-k} x_k e^{-i\omega t_k}. \tag{14}$$

In the Welch method, x_t is subdivised into possibly overlapping blocks of size N and with an overlap N_o. A Fast Fourier Transform is performed on each windowed block to extract the

Fourier component at the tidal frequency, denoted X_ω^l where l is the block index. We define

$$X_\omega^l = \sum_{k=0}^{N} x_{k+l(N-N_o)} W_k e^{-i\omega t_k}, \tag{15}$$

where W_k is a window function. By changing variable $k' = k + l(N - N_o)$, we obtain

$$X_\omega^l = e^{i\omega t_{l(N-N_o)}} \sum_{k'=l(N-N_o)}^{N+l(N-N_o)} x_{k'} W_{k'-l(N-N_o)} e^{-i\omega t_{k'}}. \tag{16}$$

Assuming that the window function is symmetrical in the middle of each block (which is verified for most windows used in the literature), i.e $W_k = W_{N-k}$, equation (16) gives

$$X_\omega^l = e^{i\omega t_{l(N-N_o)}} \sum_{k'=l(N-N_o)}^{N+l(N-N_o)} W_{N+l(N-N_o)-k'} x_{k'} e^{-i\omega t_{k'}}. \tag{17}$$

Finally, by choosing $W_k = b_k$ which sets $m = \frac{N}{2}$, relation (14) yields

$$X_\omega^l = e^{i\omega t_{l(N-N_o)}} (\mathcal{L}(x_t e^{-i\omega t}))_{\frac{N}{2}+l(N-N_o)}. \tag{18}$$

Consequently, up to a phase, the Welch method corresponds to the computation of the complex demodulated signal sampled every $N - N_o$. The phase shift cancels when computing the correlation over N_b blocks :

$$\sum_{l=0}^{N_b} X_\omega^l {X_\omega^l}^* = \sum_{l=0}^{N_b} (\mathcal{L}(x_t e^{-i\omega t}))_{\frac{N}{2}+l(N-N_o)} (\mathcal{L}^*(x_t e^{-i\omega t}))_{\frac{N}{2}+l(N-N_o)}. \tag{19}$$

The CSD can thus be obtained by computing the correlation over N_b snapshots sampled every $N - N_o$ of the complex demodulated signal, which is proving the equivalence between the two methods for appropriate numerical parameters.

As said before, it can be remarked that the window function acts as a filter in the Welch procedure, but without giving an explicit expression of the frequency band. Moreover, if we aim at studying the whole broadband field, the classical SPOD (with its single frequency interpretation when the window function is designed to only estimate a pure harmonic) requires the computation of a set of spatial modes at each discrete frequency in the peak. In comparison, BBPOD computes at only one frequency the dominant modes of the wave field. This has the drawback for the SPOD algorithm to include at each frequency a few modes of nearby frequency due to the convolution with a finite length window, leading to misinterpretation or counting the same mode several times in the reconstruction of the whole wave field. More precisely, BBPOD gathers the first SPOD mode of each frequency providing a simpler representation of the whole wave field and avoids spurious modes in the reconstruction. Another important remark is that the connection of our method with SPOD lies on the fact that the spectral peak is sufficiently narrow corresponding of a sufficiently large window in the Welch method guaranteeing a good

estimation of the CSD.

The final step is to compute the eigenvalues and eigenvectors of the CSD, estimated by complex demodulation. The complex demodulated signal at frequency ω is then decomposed on this BBPOD basis:

$$\boldsymbol{q}_d(x,y,t) = \sum_j a_j(\omega,t)\boldsymbol{\psi}_j(x,y,\omega), \tag{20}$$

with $a_j(\omega,t) = \int_\Omega \boldsymbol{q}_d^*(x,y,t)\mathbf{W}(x,y)\boldsymbol{\psi}_j(x,y,\omega)\,\mathrm{d}x\mathrm{d}y$ slowly varying coefficients.

3.2.3 Extended broadband proper orthogonal decomposition

Non-linear interactions between slow variations of the background flow and the wave induce incoherent wave contributions through triadic interactions. A major interest of BBPOD is that it allows us to study the correlations between the slow perturbations of the jet, and the incoherence of the fast wave field, by extracting the slowly varying complex demodulated amplitudes. To that end, we propose to apply the concept of EPOD in the framework of BBPOD. EPOD, originally presented in Boree (2003), enables to identify the part of a target field correlated with a given POD mode. The target field we first consider is the balanced motion obtained by low-pass filtering. The p-th extended POD mode of the slow motion $\boldsymbol{q}^j$ correlated to the p-th BBPOD coefficient of the wave a_p^ω is defined by :

$$\boldsymbol{\chi}_p^j = \frac{\mathbb{E}(\boldsymbol{q}^j a_p(\omega))}{\lambda_p(\omega)}, \tag{21}$$

where the expectation operator is a temporal average over snapshots. The mode $\boldsymbol{\chi}_p^j$ will be referred to as *direct EPOD*, and $a_p(\omega)\boldsymbol{\chi}_p^j$ represents the part of the jet correlated with the p-th broadband POD coefficient of the wave.

Complementary to direct EPOD, we define as well an *inverse EPOD*, applying BBPOD for $\omega = 0$, thus obtaining an orthonormal basis representative of the jet variability, and considering the complex demodulated of the wave contribution $\boldsymbol{q}_d$ as the target field. In this situation, we identify the contribution of the incoherent wave field correlated with the BBPOD coefficients of the jet noted $a_p(\omega = 0)$. Therefore, in the following direct EPOD refer to jet modes while inverse EPOD refer to wave modes.

4 Results

This section details the numerical results carried out in this work. The goal is to understand the non-linear interactions between the balanced motion and the wave field by means of the methods presented in section 3, that will extract the correlations between the two dynamics.

Figure 2 shows the real part of the first three energy-scaled BBPOD modes at the tidal frequency, sorted by decreasing energy (4). Specifically here, we plot the scaled quantities $\sqrt{\lambda_j}\psi_j$ to highlight their respective energy contribution, but the analysis was performed with the normalized modes. To define the low pass filter $\mathcal{L}$, a fourth order Butterworth filter has been taken with

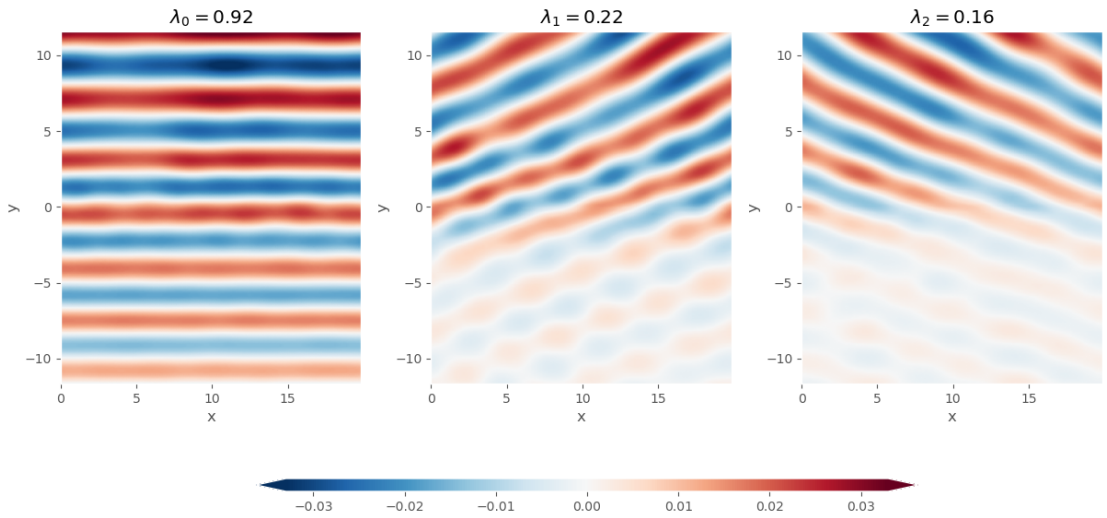

Figure 2: Real part of the first three energy-scaled BBPOD modes $\sqrt{\lambda_j}\psi_j$ associated with u at the tidal frequency. Sponge regions are not shown.

a frequency cut-off equals to the typical frequencies of the jet, such that the whole wave-field scattered by the jet is captured. The first mode containing the most energy corresponds to the coherent wave field, that is defined here as the part of the wave correlated to the tidal forcing and thus phase-locked in time, since it corresponds to the time-average of the complex-demodulated signal. Other modes account then for the incoherent structures as space-time decorrelated of the mean. They show deflections in opposite direction, with mode-number $m_x = \pm 2$, and with meridional mode-number m_y expected to be determined by the dispersion relation (3) and the structure of the jet (see Bühler 2014)). This is a consequence of the homogeneity in the zonal direction, guaranteed by our idealised set-up, which makes SPOD modes equal to Fourier modes in x.

Table 1 shows the normalised energy contained in the first five BBPOD modes and in the incoherence field. It is computed for the domain without sponge regions noted $\Omega = [0, 20] \times [-12, 12]$ and for the subset $\Omega^N = [0, 20] \times [-2, 12]$ representing the region of incoherences.

In the total domain, the coherent plane wave accounts for 57.35 % of the energy and the first three modes 81 % of the energy. This shows that linear effects dominate the wave propagation, because we are in a configuration for which incoherence is relatively weak. As explained in Ward and Dewar (2010), a more energetic jet interacting with a tide with higher frequency would result in a more energetic incoherent wave field for a RSW simulation. As expected, incoherent modes have nearly all their energy in the upper part while it is rather equally distributed for the coherent mode. In this region, incoherences are dominant due to non-linearities in the center of the domain, which leads to an increase of the amplitude of the modes with y, even though the coherent mode still contains the most energy. Figure 3 shows the energy contained in the reconstructed incoherent wave field in terms of cumulative energy. The first two incoherent modes account for 58 % of the total incoherent energy. For 6 modes, 80 % of the energy is

Table 1: Normalized energy of the first 5 modes shown in percentage. Computed in Ω and in Ω^N. Each eigenvalue is divided by the total variance in Ω at the tidal frequency $\sum_j \lambda_j^{\Omega}(f)$.

Mode	Ω	Ω^N
1	57.35	29.04
2	13.81	12.98
3	9.86	9.51
4	3.86	3.77
5	2.34	2.13
Sum of Incoherence	42.64	37.91

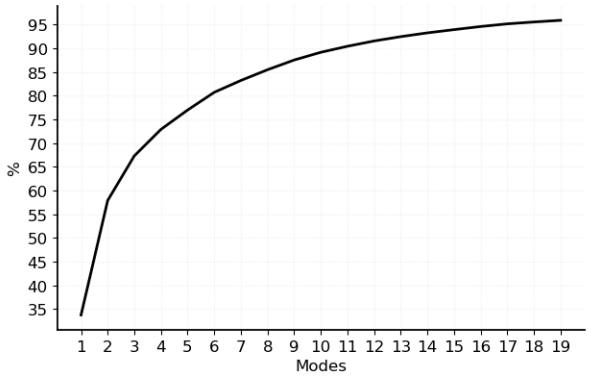

Figure 3: Cumulative energy $\sum_{j=1}^{N} \lambda_j(\omega) / \sum_{j=1}^{+\infty} \lambda_j(\omega)[\%]$ contained in the reconstruction of the incoherent field by BBPOD modes.

recovered in the reconstruction. The cumulative energy can be understood as a normalized RMSE measuring the accuracy of the basis to reconstruct the true incoherent wave field $\boldsymbol{q}_{inc}$ according to $\frac{\mathbb{E}(\|\boldsymbol{q}_{inc} - \sum_{j=1}^{N}(\boldsymbol{q}_{inc}, \boldsymbol{\psi}_j)\boldsymbol{\psi}_j\|^2_{L^2(\Omega)})}{\mathbb{E}(\|\boldsymbol{q}_{inc}\|^2_{L^2(\Omega)})} = 1 - \sum_{j=1}^{N} \lambda_j(\omega) / \sum_{j=1}^{+\infty} \lambda_j(\omega)$. It can be remarked that spatial coherence can be computed with the coherence function γ through the CSD.

A SPOD decomposition was also performed in Egbert and Erofeeva (2021) for a realistic HYCOM simulation. Similar results were found for the energy captured by the SPOD modes at the M2 frequency, which is similar to our forcing frequency. This encourages to extend this analysis to a more realistic simulation.

Figure 4 depicts the direct EPOD modes of the balanced motion, correlated with the BBPOD modes of the wave. The modes are weighted as explained before. The first extended mode is showing that the part of the jet correlated with the coherent field is the stationary mean flow, which connects the first order statistic of both dynamics. This results is the expression of the linear propagation of the incident wave through the mean flow (in time and in the x-direction). The second and third EPOD modes represent the meanders of the jet, consisting of a vortex train. The modes are defined up to a complex constant. We can see that $\boldsymbol{\chi}_2^j$ is approximately

proportional to $\boldsymbol{\chi}_3^j$, suggesting that meandering of the jet generates eastward and westward propagating incoherent perturbations.

The opposite procedure is done next by inverse EPOD. Figure 5 shows the leading three jet (energy-scaled) BBPOD modes associated with $\omega = 0$ and the associated EPOD modes of the wave. As in direct EPOD, the first mode is showing the correlation between the mean of both dynamics. For the second and third modes, BBPOD shows jet meandering structures identical to the direct EPOD modes (up to a phase). However, their associated inverse EPOD indicate a standing wave corresponding to the sum of the two direct broadband POD modes that represent left and right deflections, expressing the fact that the EPOD and BBPOD association is not bijective. A given meander will give rise to a wave deflected eastward nearly as much as a wave deflected westward, and their relative contribution is not possible to predict, but the present result suggests that an approximately equal repartition would constitute a fair estimate.

Globally, we can infer that the most energetic triadic interactions between the jet and the plane wave are caused by meandering structures of the jet generating an incoherent field of the form of a standing wave in the zonal direction x and propagating northward. The rising of a standing wave suggests in average an equal distribution of the eastward and westward propagating modes. This gives nice perspectives of incorporating this methodology in the context of data assimilation to estimate the incoherent wave field with some knowledge of the slow balanced flow through triadic interactions.

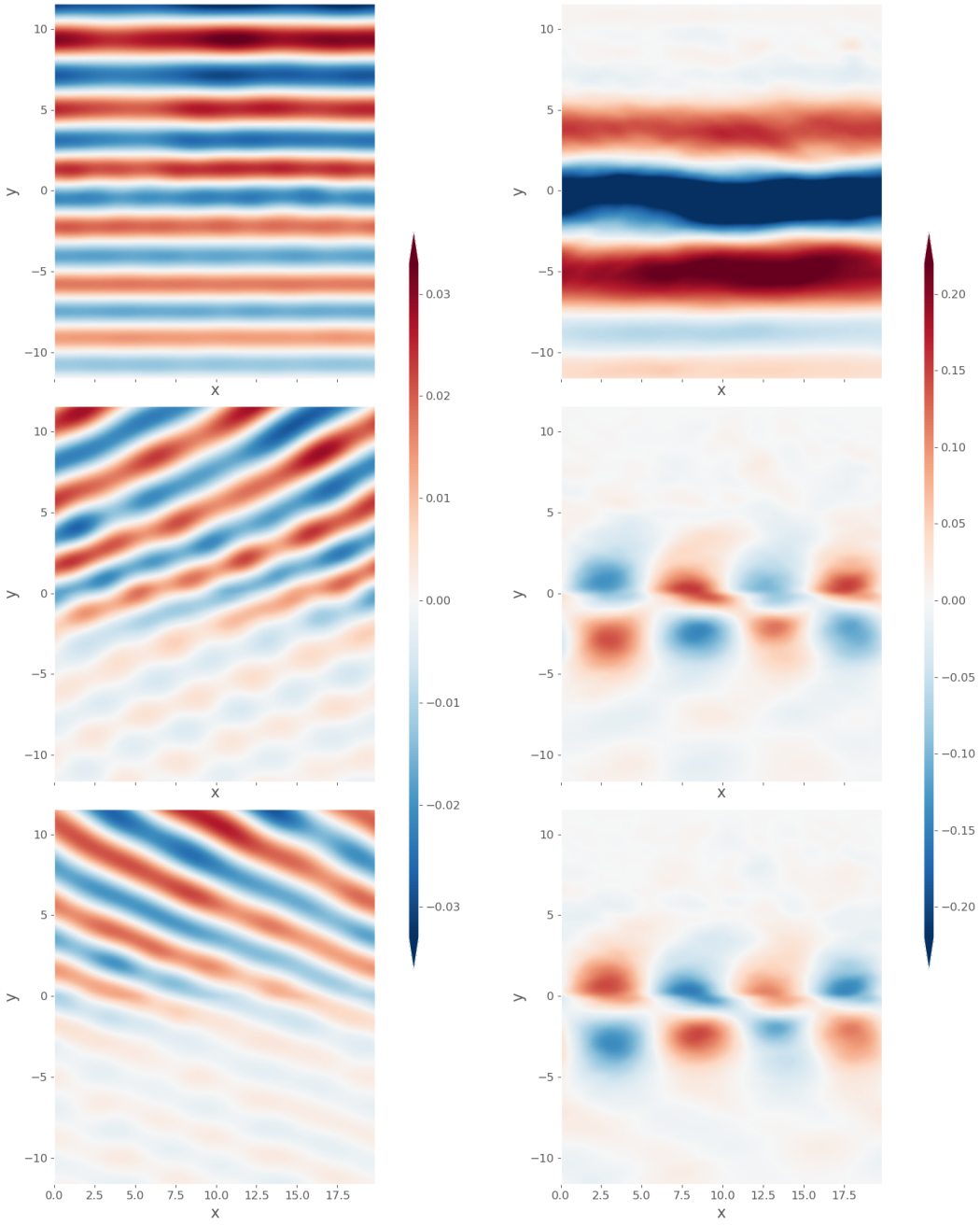

Figure 4: On the left column are presented the real part of the first three BBPOD modes of u at the tidal frequency. On the last column are the corresponding direct EPOD modes of u. Modes are scaled as follows: $\sqrt{\lambda_j}\psi_j$.

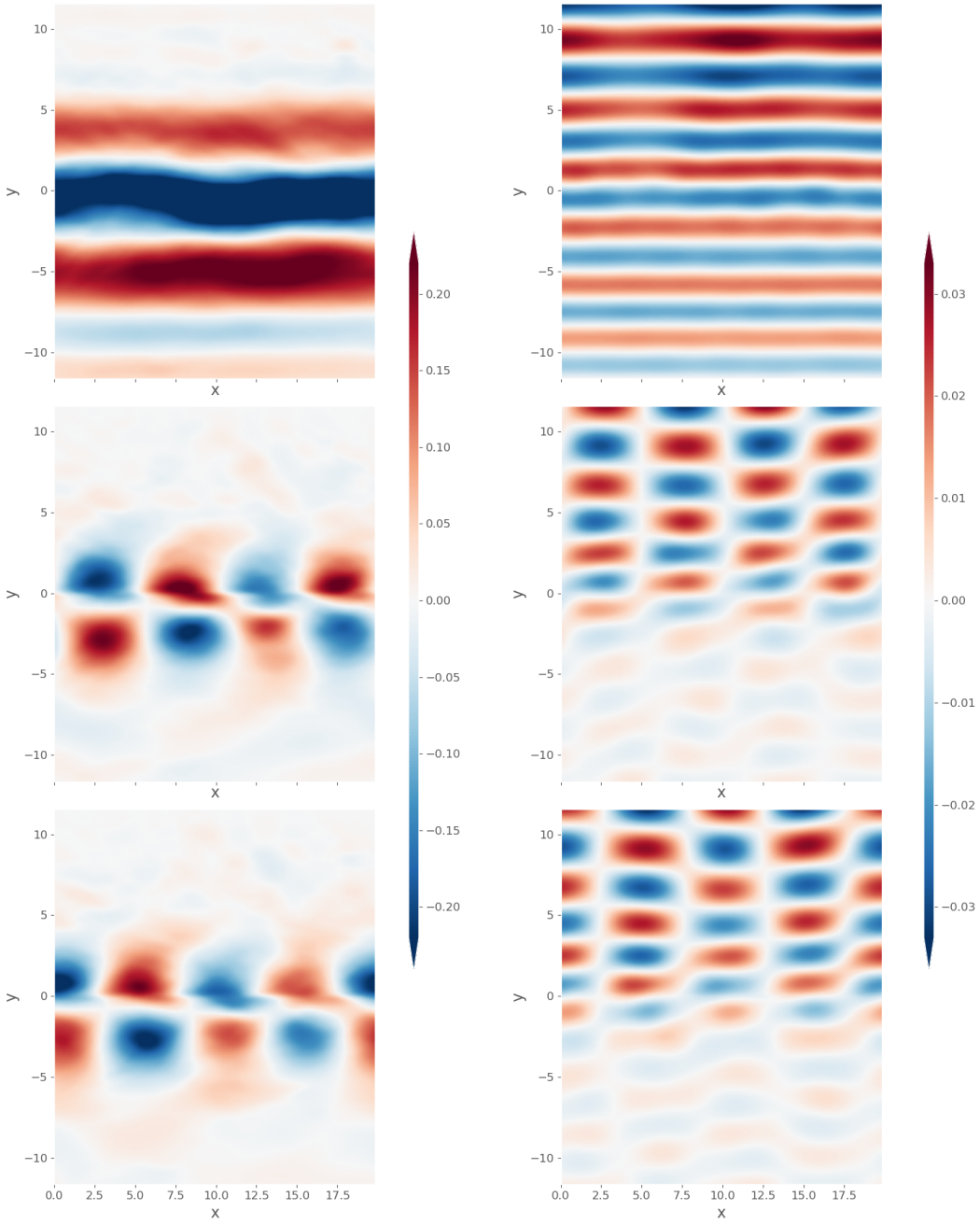

Figure 5: On the first column are presented the first three BBPOD modes of u of the jet. On the last column are the associated inverse EPOD modes of u. Modes are scaled as follows : $\sqrt{\lambda_j}\ \psi_j$.

5 Summary and Perspectives

This study investigates the correlated processes at stake within the non-linear interactions of a plane wave propagating through a meso-scale oceanic current. For that purpose, the method of broadband POD is introduced and connected to extended POD. A first methodological point is done to show that BBPOD is equivalent to the common Welch method to estimate the cross spectral density matrix, to which SPOD are the eigenfunctions. More importantly for our study, connecting these two methods allows us to understand that the most energetic features of the wave are obtained by triadic interactions with the most energetic features of the jet. In our idealised configuration, the wave is deflected in both directions by a given meander. The spatial periodicity of the meander sets the zonal deflections, giving us clearer insight on the BBPOD of the wave knowing only the extended modes of the jet. This method can be seen as complementary to methods based on the bispectrum to detect triadic interactions in the data. Here we have an a priori on the nature of the interactions, between a low frequency jet and a fast wave field, allowing to study directly their correlations and to propose a methodology well suited for reconstruction. In a future work, we intend to examine the sensitivity of the results to other jet or wave configurations, and even to richer models. Studying the implications of these methods to reconstruct by correlation the internal wave field by the knowledge of the instantaneous slow motion is also envisaged for data assimilation problematics, either by direct estimation, or for learning an observation operator associated with a Galerkin model defined in the BBPOD space.

References

Boree, Jacques (Aug. 2003). "Extended proper orthogonal decomposition: A tool to analyse correlated events in turbulent flows". In: *Experiments in Fluids* 35, pp. 188–192. DOI: 10.1007/s00348-003-0656-3.

Brunet, Gilbert and Robert Vautard (1996). "Empirical Normal Modes versus Empirical Orthogonal Functions for Statistical Prediction". In: *Journal of Atmospheric Sciences* 53.23, pp. 3468–3489. DOI: 10.1175/1520-0469(1996)053<3468:ENMVEO>2.0.CO;2.

Bühler, Oliver (2014). *Waves and Mean Flows*. 2nd ed. Cambridge Monographs on Mechanics. Cambridge University Press. DOI: 10.1017/CBO9781107478701.

Burns, Keaton J., Geoffrey M. Vasil, Jeffrey S. Oishi, Daniel Lecoanet, and Benjamin P. Brown (Apr. 2020). "Dedalus: A flexible framework for numerical simulations with spectral methods". In: *Physical Review Research* 2.2, 023068, p. 023068. DOI: 10.1103/PhysRevResearch.2.023068.

Dunphy, Michael, Aurelien Ponte, Patrice Klein, and Sylvie Le Gentil (2017). "Low-mode internal tide propagation in a turbulent eddy field". In: *Journal Of Physical Oceanography* 47.3. Ed. by Amer Meteorological Soc, pp. 649–665. DOI: https://doi.org/10.1175/JPO-D-16-0099.1.

Egbert, G. D. and S. Y. Erofeeva (2021). "An Approach to Empirical Mapping of Incoherent Internal Tides With Altimetry Data". In: *Geophysical Research Letters* 48.24, e2021GL095863. DOI: https://doi.org/10.1029/2021GL095863.

Godfrey, Michael D. (1965). "An exploratory study of the bi-spectrum of economic time series". In: *Journal of The Royal Statistical Society Series C-applied Statistics* 14, pp. 48–69.

Karban, U., E. Martini, A.V.G. Cavalieri, L. Lesshafft, and P. Jordan (2022). "Self-similar mechanisms in wall turbulence studied using resolvent analysis". In: *Journal of Fluid Mechanics* 939, A36. DOI: 10.1017/jfm.2022.225.

Loève (1955). *Probability theory*. Van Nostrand.

Lumley, J.L (1967). "The Structure of Inhomogeneous Turbulent Flows". In: *Atmospheric Turbulence and Radio Wave Propagation*. Ed. by A.M. Yaglom and V.I. Tartarsky, pp. 166–177.

Ochoa, José, Julio Sheinenbaum, and Aleph Jiménez (2011). "Lateral Friction in Reduced-Gravity Models: Parameterizations Consistent with Energy Dissipation and Conservation of Angular Momentum". In: *Journal of Physical Oceanography* 41.10, pp. 1894–1901. DOI: 10.1175/2011JPO4599.1.

Ponte, A. L. and P. Klein (2015). "Incoherent signature of internal tides on sea level in idealized numerical simulations". In: *Geophysical Research Letters* 42.5, pp. 1520–1526. DOI: https://doi.org/10.1002/2014GL062583.

Richman, James G., Brian K. Arbic, Jay F. Shriver, E. Joseph Metzger, and Alan J. Wallcraft (2012). "Inferring dynamics from the wavenumber spectra of an eddying global ocean model with embedded tides". In: *Journal of Geophysical Research: Oceans* 117.C12. DOI: https://doi.org/10.1029/2012JC008364.

Savva, Miles and Jacques Vanneste (Dec. 2018). "Scattering of internal tides by barotropic quasigeostrophic flows". In: *Journal of Fluid Mechanics* 856, pp. 504–530. DOI: 10.1017/jfm.2018.694.

Schmidt, Oliver T. and Tim Colonius (2020). "Guide to Spectral Proper Orthogonal Decomposition". In: *AIAA Journal* 58.3, pp. 1023–1033. DOI: 10.2514/1.J058809.

Towne, Aaron, Oliver T. Schmidt, and Tim Colonius (2018). "Spectral proper orthogonal decomposition and its relationship to dynamic mode decomposition and resolvent analysis". In: *Journal of Fluid Mechanics* 847, pp. 821–867. DOI: 10.1017/jfm.2018.283.

Ward, Marshall L. and William K. Dewar (2010). "Scattering of gravity waves by potential vorticity in a shallow-water fluid". In: *Journal of Fluid Mechanics* 663, pp. 478–506. DOI: 10.1017/S0022112010003721.

Welch, P. (1967). "The use of fast Fourier transform for the estimation of power spectra: A method based on time averaging over short, modified periodograms". In: *IEEE Transactions on Audio and Electroacoustics* 15.2, pp. 70–73. DOI: 10.1109/TAU.1967.1161901.